Precommitment low-level *Neurog3* expression defines a long-lived mitotic endocrine-biased progenitor pool that drives production of endocrine-committed cells

Matthew E. Bechard,[1] Eric D. Bankaitis,[1] Susan B. Hipkens,[1,2] Alessandro Ustione,[2,3] David W. Piston,[2,3] Yu-Ping Yang,[1] Mark A. Magnuson,[1,2] and Christopher V.E. Wright[1]

[1]Vanderbilt University Program in Developmental Biology, Department of Cell and Developmental Biology, Vanderbilt Center for Stem Cell Biology, Vanderbilt University School of Medicine, Nashville, Tennessee 37232, USA; [2]Department of Molecular Physiology and Biophysics, Vanderbilt University School of Medicine, Nashville, Tennessee 37232, USA

The current model for endocrine cell specification in the pancreas invokes high-level production of the transcription factor Neurogenin 3 (Neurog3) in Sox9$^+$ bipotent epithelial cells as the trigger for endocrine commitment, cell cycle exit, and rapid delamination toward proto-islet clusters. This model posits a transient *Neurog3* expression state and short epithelial residence period. We show, however, that a *Neurog3*$^{TA.LO}$ cell population, defined as *Neurog3* transcriptionally active and Sox9$^+$ and often containing nonimmunodetectable Neurog3 protein, has a relatively high mitotic index and prolonged epithelial residency. We propose that this endocrine-biased mitotic progenitor state is functionally separated from a pro-ductal pool and endows them with long-term capacity to make endocrine fate-directed progeny. A novel BAC transgenic *Neurog3* reporter detected two types of mitotic behavior in Sox9$^+$ *Neurog3*$^{TA.LO}$ progenitors, associated with progenitor pool maintenance or derivation of endocrine-committed Neurog3^{HI} cells, respectively. Moreover, limiting *Neurog3* expression dramatically increased the proportional representation of Sox9$^+$ *Neurog3*$^{TA.LO}$ progenitors, with a doubling of its mitotic index relative to normal *Neurog3* expression, suggesting that low *Neurog3* expression is a defining feature of this cycling endocrine-biased state. We propose that Sox9$^+$ *Neurog3*$^{TA.LO}$ endocrine-biased progenitors feed production of Neurog3^{HI} endocrine-committed cells during pancreas organogenesis.

[*Keywords*: *Neurog3*; progenitor; endocrine-biased; mitotic]

Supplemental material is available for this article.

Received May 27, 2016; revised version accepted August 3, 2016.

During mammalian organogenesis, lineage specification and commitment involve passage through distinct progenitor/precursor states that rely on different combinations and levels of transcription factors (Wilkinson et al. 2013; Cano et al. 2014). In the current model of pancreatic endocrine cell formation, *Neurogenin3* (*Neurog3*) expression in the epithelium rapidly progresses to a high-level production of protein (Neurog3^{HI}) that leads to endocrine fate commitment, cell cycle exit, and delamination toward proto-islet clusters. Meta-analysis of published literature (see below), however, is suggestive of a broader pattern of lower-level *Neurog3* expression across the epithelium that is substantially more prevalent than the actively delaminating endocrine-committed Neurog3^{HI} population. The present study is focused on determining whether this low-*Neurog3*-expressing subpopulation represents the early-phase expression in post-mitotic cells on their way to becoming Neurog3^{HI} cells or endocrine fate-biased but uncommitted mitotic cells that have self-maintaining progenitor characteristics.

Pancreas organogenesis is divided into a primary transition and secondary transition (Pan and Wright 2011). During the primary transition (embryonic day 9.5 [E9.5] to E12.5), multipotent progenitor cells undergo apical polarization, forming microlumens that then coalesce to generate an epithelial plexus. Within this epithelial plexus, progenitor cells (around E12.5) segregate into "tip" and "trunk" domains. In the short-term, tip domains

[3]Present address: Cell Biology and Physiology, Washington University School of Medicine, St. Louis, MO 63110, USA.
Corresponding author: chris.wright@vanderbilt.edu
Article published online ahead of print. Article and publication date are online at http://www.genesdev.org/cgi/doi/10.1101/gad.284729.116.

transiently retain their multipotency to form acinar, duct, and endocrine lineages before transitioning to a proacinar state. The trunk domain, a primary component of the epithelial plexus, consists of a pool of duct/endocrine bipotential Sox9$^+$ Hnf1b$^+$ Nkx6.1$^+$ cells (Seymour et al. 2007; Solar et al. 2009). Recently, we reported that distinct modes of epithelial morphogenesis in the peripheral versus core regions of the developing pancreas work in concert to generate the final "epithelial tree" of the mature pancreas (Bankaitis et al. 2015). In the core, the epithelial plexus remodels into mature ductal tissues via growth and expansion (E12.5–E15.5) followed by plexus-to-duct transformation (E16.5–E18.5) (Bankaitis et al. 2015). Although the plexus is progressively lost, remodeling into "mature" ducts and ductal branches, it is present during all stages of the secondary transition. Even at late gestation, plexus-state epithelium generates as many endocrine cells as earlier in the secondary transition, suggesting that the plexus represents a primary endocrine progenitor niche (Bankaitis et al. 2015). Within the trunk plexus-state epithelium, the transcription factor Neurog3 is a key trigger factor for endocrine lineage commitment. Expressed in a subset of the Sox9$^+$ duct/endocrine bipotent progenitors, high Neurog3 protein levels activate the expression of general proendocrine transcription factor genes (*NeuroD1*, *Insm1A*, and *Isl1*) followed by those for endocrine lineage-specific factors (*Pax4*, *Nkx2.2*, and *Arx*). *Neurog3*^{NULL} mice show a vast deficiency in endocrine cell production and a near absence at birth (Gradwohl et al. 2000; Johansson et al. 2007). An inducible *Neurog3* overexpression system showed an endoderm-autonomous competence for Neurog3^{HI} cells to produce mostly α (glucagon-producing) cells in early pancreas organogenesis (E8.75–E12.5), with the ability to produce β cells (and other endocrine cells in lesser number) arising in the secondary transition (Johansson et al. 2007). A large-scale clonal analysis demonstrated that the majority of Neurog3^{HI} cells each represents a unipotent precursor of a single hormone-expressing endocrine cell type (Desgraz and Herrera 2009); for example, insulin or glucagon. These studies show that the epithelial competence to produce the various endocrine hormone-secreting cells switches over time and that Neurog3 is necessary and sufficient for endocrine lineage commitment.

The transition from *Neurog3* activation to an endocrine-committed Neurog3^{HI} state is thought to occur rapidly, predicting a low epithelial residency period for *Neurog3*-expressing cells. Our closer examination of the primary data in several studies, however, revealed evidence that could be interpreted as opposing this view. First, low-level *Neurog3* expression within the secondary transition pancreatic epithelium seems widespread. Either *Neurog3*$^{BAC.Cre}$;*R26R* lineage tracing or a *Neurog3*$^{EGFP/+}$ knock-in reporter detects a large number of intraepithelial cells that potentially represent cells in a *Neurog3*-expressing pre-endocrine-committed state (Zhang et al. 2009; Wang et al. 2010; Bankaitis et al. 2015). In the study by Villasenor et al. (2008), *Neurog3* mRNA detection also suggests a *Neurog3*-expressing epithelial population that is broader than that visualized by Neurog3 immunodetection. Furthermore, in situ RNA hybridization with a cocktail of endocrine-specific probes, including *Neurog3*, showed a substantial occupancy of the epithelial trunk domain by putative endocrine progenitors or precursors (Zhou et al. 2007). Multiple studies report a small but significant number of nonendocrine cells as generated from *Neurog3*-expressing epithelial cells, suggesting that, in a minority of cases, activating *Neurog3* expression does not unequivocally instruct endocrine commitment (Schonhoff et al. 2004; Wang et al. 2010). We propose that these studies suggest an intraepithelial subpopulation of *Neurog3*-expressing cells of significant interest in that it might represent a distinct, possibly mitotic, endocrine-biased progenitor state localized to or highly enriched within plexus-state epithelium, which feeds production of endocrine-committed cells during the secondary transition.

These studies prompted our investigation of this endocrine-biased *Neurog3*-expressing epithelial population, focusing on the hypothesis that it does represent a mitotic feeder population. Moreover, we also report a novel *Neurog3* BAC transgenic reporter sensitive enough to mark low-level *Neurog3*-expressing cells, allowing a deeper analysis of endocrine specification and commitment. We present several lines of evidence that *Sox9*-expressing, *Neurog3* transcriptionally active (*Neurog3*^{TA}) cells with low or even immunologically undetectable Neurog3 protein (referred to here as *Neurog3*$^{TA.LO}$ cells) in fact do represent a mitotic progenitor state that is distinguishable from endocrine-committed Neurog3^{HI} cells and Sox9$^+$ *Neurog3*$^-$ pro-duct progenitors. Our real-time analysis shows that Sox9$^+$ *Neurog3*$^{TA.LO}$ progenitors undergo divisions that either maintain the *Neurog3*$^{TA.LO}$ progenitor pool or generate endocrine-committed Neurog3^{HI} cells. Furthermore, genetically limiting *Neurog3* expression increased the proliferation and significantly expanded the proportional representation of the Sox9$^+$ *Neurog3*$^{TA.LO}$ population. Our findings support a new model in which endocrine specification is driven by this novel Sox9$^+$ *Neurog3*$^{TA.LO}$ endocrine-biased progenitor pool, significantly advancing our understanding of endocrine cell ontogeny. We discuss potential parallels with the Neurog2-based regulation of the neural progenitor state versus neural specification. We propose that identifying the *Neurog3*$^{TA.LO}$ condition should focus attention on this state as being where intercellular signaling and intrinsic gene regulatory networks converge to regulate *Neurog3* expression, control the balance between progenitor maintenance and endocrine specification/commitment, and perhaps identify an early intraepithelial stage at which hormone-specific lineage allocation might occur.

Results

Mitotic Sox9$^+$ Neurog3 protein-low cells are maintained throughout the secondary transition

To study the initial phases of *Neurog3* expression, we examined Neurog3 protein levels in cells located within or outside the epithelium at E12.5, E14.5, and E16.5. Using Sox9 and Muc1 to mark epithelial cells and their lumenal

surface, respectively, we observed two discernable states of *Neurog3* expression: a Neurog3 protein-low (Neurog3^{pLO}) Sox9$^+$ Muc1$^+$ state and a Neurog3 protein-high (Neurog3^{pHI}) state that is largely Sox9$^-$ and Muc1$^-$ (Fig. 1A,B). Because we describe several distinct *Neurog3*-positive populations, for clarity, we list the nomenclature used for each and the associated cell state in Supplemental Table S1. Comparing the Neurog3 immunofluorescence signal intensities showed that Neurog3 protein levels in epithelial Sox9$^+$ Muc1$^+$ Neurog3 protein-positive (Neurog3$^{Protein+}$) cells were fivefold lower than Neurog3 protein levels in delaminated Sox9$^-$ Muc1$^-$ Neurog3$^{Protein+}$ cells at E12.5 and threefold lower for the same comparison at E14.5 (Fig. 1C). Although an avidin–biotin amplification method was used to detect Neurog3, similar results were observed with nonamplifying indirect immunofluorescence (data not shown). The certainty of the Neurog3 low-level protein signal was determined by side-by-side comparison of wild-type and *Neurog3*^{null} tissue (with no signal observed in null tissue) (Supplemental Fig. S1, A vs. B) and location over DAPI$^+$ nuclei. To evaluate the possible progenitor to precursor relationship between the Sox9$^+$ Neurog3^{pLO} and Sox9$^-$ Neurog3^{pHI} populations, respectively, their proportional representations with respect to each other were quantified at E12.5, E14.5, and E16.5 (Fig. 1D). One would expect the number of Neurog3^{pLO} relative to Neurog3^{pHI} cells to be largely equal during the secondary transition if Sox9$^+$ Neurog3^{pLO} cells represented the early-stage upsweep of expression during the rapid progression from *Neurog3* activation to Neurog3^{pHI} in each endocrine-committing cell. At E12.5, however, Sox9$^+$ Neurog3^{pLO} cells outnumbered Neurog3^{pHI} cells by a small but significant margin (Fig. 1D), while stages after E12.5 exhibited a shift in favor of Sox9$^-$ Neurog3^{pHI} and away from Sox9$^+$ Neurog3^{pLO} cells (Fig. 1D). These data are consistent with Sox9$^+$ Neurog3^{pLO} cells functioning as a progenitor pool that gives rise to Neurog3^{pHI} endocrine precursors. To determine whether the Sox9$^+$ Neurog3^{pLO} population varied during the secondary transition, their number as a proportion of the entire Sox9$^+$ epithelium was quantified between E12.5 and E16.5. Despite a decrease from E12.5 to E14.5, the Sox9$^+$ Neurog3^{pLO} population remained at a similar level between E14.5 and E16.5 (Supplemental Fig. S2). Although the numbers of Sox9$^+$ Neurog3^{pLO} cells seem quite low if scored relative to the entire epithelium, their representation is likely much higher within the central epithelial plexus (further supporting evidence is presented below), in which the majority of *Neurog3*$^+$ cells reside and which produces endocrine cells with a relatively constant yield between E14.5 and E16.5 (Bankaitis et al. 2015). Because we suspected that the Sox9$^+$ Neurog3^{pLO} pool functions as a cycling progenitor population, we tested its proliferative index relative to endocrine-committed Neurog3^{pHI} cells. Detecting phospho-histone H3 (pHH3) to mark cell cycle M phase, over DAPI$^+$ nuclei, substantial numbers of intraepithelial pHH3$^+$ Neurog3^{pLO} cells were found at E12.5 and E14.5 (Fig. 1E–H). Although, above, we used Sox9 to mark intraepithelial cells, the fact that both Sox9 and pHH3 antibodies were raised in rabbits prompted the use of Muc1 (an apical surface marker) and DAPI to identify epithelial cells with a definitive apical lumen-contacting surface. Quantification revealed 11.5% ± 1.7% of Muc1$^+$ Neurog3^{pLO} cells as pHH3$^+$ at E12.5 versus 7.6% ± 1.8% at E14.5 (Fig. 1I). Consistent with previous studies (Gu et al. 2002; Desgraz and Herrera 2009), Sox9$^-$ Neurog3^{pHI} cells had very few pHH3$^+$ cells and thus were largely post-mitotic (Fig. 1I). Quantifying immunofluorescence signal intensities in Muc1$^+$ Neurog3$^{Protein+}$ pHH3$^+$ cells versus Muc1$^-$ Neurog3$^{Protein+}$ pHH3$^-$ cells at E12.5 and E14.5 confirmed that intraepithelial pHH3$^+$ Neurog3$^{Protein+}$ cells were in the Neurog3^{pLO} state (Fig. 1J). These data together support the idea that the intraepithelial Neurog3^{pLO} condition is an appreciably mitotic progenitor state that, as a population, perdures during the secondary transition. We postulate that the greater number and mitotic index of intraepithelial Neurog3^{pLO} cells at E12.5 (Fig. 1D,I) are possibly connected to the expansion of the plexus niche as the pancreatic epithelium enters the secondary transition period (Bankaitis et al. 2015).

Neurog3 *transcriptional activity marks a mitotic Sox9*$^+$ Neurog3$^+$ *endocrine progenitor population*

As discussed above, previous reports showed *Neurog3* mRNA expression to be broader than Neurog3 protein and to include intraepithelial cells. To investigate intraepithelial *Neurog3*-expressing cells further, we used the *Neurog3*$^{BAC.Cre}$ transgene (Schonhoff et al. 2004) to drive *R26R*^{EYFP} recombination to mark *Neurog3*^{TA} cells. Analysis at E14.5 revealed a heterogeneous pattern of EYFP-labeled Sox9$^+$ *Neurog3*^{TA} cells marked for having entered a *Neurog3*-expressing state (Supplemental Fig. S3). In peripheral regions of the pancreas, the proportion of EYFP-labeled Sox9$^+$ *Neurog3*^{TA} intraepithelial cells was as low as 5%–8%, while in central plexus-state regions, the proportional representation was locally as high as 54% (Supplemental Fig. S3). These results are consistent with previous work showing that *Neurog3*-expressing cells are mostly derived from the central plexus state and much less from peripheral regions comprising mostly duct and ductal branches (Bankaitis et al. 2015). Quantification of central plexus regions showed an overall proportional representation of 24% ± 2.4% ($N = 5$) for EYFP-labeled Sox9$^+$ *Neurog3*^{TA} cells among all Sox9$^+$ cells. Endocrine commitment is thought to occur rapidly after *Neurog3* activation, triggering *Sox9* down-regulation, *Neurog3* up-regulation, and epithelial delamination. However, within the Sox9$^+$ EYFP-labeled *Neurog3*^{TA} population, we consistently identified a number of scattered cells with a higher EYFP signal (Supplemental Fig. S3). We speculate that, following activation of *Neurog3* expression, some Sox9$^+$ *Neurog3*^{TA} cells remain intraepithelial for a prolonged period before moving to commitment delamination and thus accumulate more EYFP. Notably, the majority of EYFP-labeled Sox9$^+$ *Neurog3*^{TA} cells within these plexus regions were clustered and not fully interspersed with EYFP-negative cells. We propose that it is highly unlikely that all of these clustered cells are

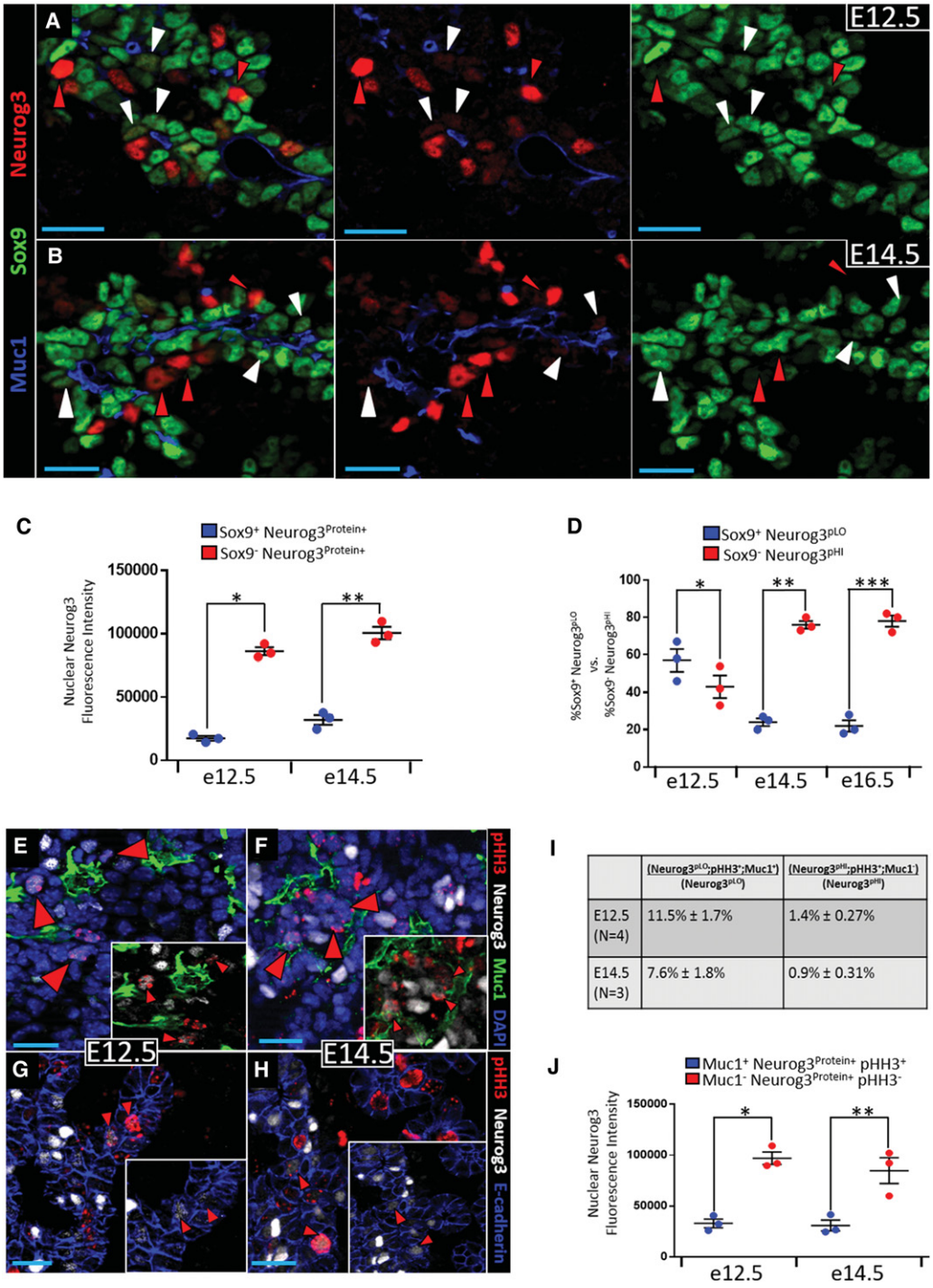

	(Neurog3^{pLO};pHH3^{+};Muc1^{+}) / (Neurog3^{pLO})	(Neurog3^{pHI};pHH3^{+};Muc1^{-}) / (Neurog3^{pHI})
E12.5 (N=4)	11.5% ± 1.7%	1.4% ± 0.27%
E14.5 (N=3)	7.6% ± 1.8%	0.9% ± 0.31%

Figure 1. The Neurog3$^{Protein+}$ population is comprised of mitotic Neurog3^{pLO} and post-mitotic Neurog3^{pHI} cells. E12.5 (*A*) and E14.5 (*B*) pancreatic epithelium showing Muc1, Sox9, and Neurog3. White and red arrowheads indicate Sox9^{+} Muc1^{+} Neurog3^{pLO} cells and Sox9^{-} Muc1^{-} Neurog3^{pHI}, respectively. (*C*) Average fluorescence intensity of nuclear Neurog3 signal in Sox9^{+} Neurog3$^{Protein+}$ versus Sox9^{-} Neurog3$^{Protein+}$ cells. $n = 9$ cryosections; $N = 3$ pancreata at E12.5 and E14.5. (*) $P = 2 \times 10^{-5}$; (**) $P = 0.0002$. (*D*) Percentage of Sox9^{+} Neurog3^{pLO} versus Sox9^{-} Neurog3^{pHI} cells at E12.5 ($n = 1114$; $N = 3$), E14.5 ($n = 3797$; $N = 3$), and E16.5 ($n = 4374$; $N = 3$). (*) $P = 0.0895$; (**) $P = 3 \times 10^{-5}$; (***) $P = 0.0001$. E12.5 (*E*,*G*) and E14.5 (*F*,*H*) pancreatic epithelium showing pHH3, Neurog3, Muc1, and DAPI or pHH3, Neurog3, and E-cadherin. Red arrowheads indicate intraepithelial pHH3^{+} Neurog3^{pLO} cells. (*I*) Mitotic index of Muc1^{+} Neurog3^{pLO} cells versus Muc1^{-} Neurog3^{pHI} cells at E12.5 ($n = 1546$) and E14.5 ($n = 10080$). (*J*) Average fluorescence intensity of nuclear Neurog3 signal in Muc1^{+} Neurog3$^{Protein+}$ pHH3^{+} cells versus Muc1^{-} Neurog3$^{Protein+}$ pHH3^{-} cells at E12.5 and E14.5, calculated as in *C*. Data are mean ± SEM. (*) $P = 0.0005$; (**) $P = 0.0087$.

concurrently transitioning to the *Neurog3*^{HI} state. This observation thus supports the notion that low-level *Neurog3* activation in Sox9$^+$ cells, combined with a substantial residence period, leads to a sizeable intraepithelial representation of this cell population. It should be remembered that there is eventually only a tiny final contribution of EYFP-labeled *Neurog3*$^{BAC.Cre}$ traced cells to mature duct fates (~1%) (Schonhoff et al. 2004), meaning that essentially all of these "transiently intraepithelial" cells do eventually progress to endocrine commitment.

Within these EYFP-labeled Sox9$^+$ *Neurog3*^{TA} cells, in addition to some containing detectable but low-level Neurog3 protein (*Neurog3*$^{TA.pLO}$), many more had none detectable (*Neurog3*$^{TA.pUD}$) (Fig. 2A,B; Supplemental Table S1). The proliferation marker pHH3 revealed numerous mitotic intraepithelial *Neurog3*$^{TA.pLO}$ (defined here as Muc1$^+$ lumen-contacting) (presumably equivalent to those in Fig. 1E–H) as well as *Neurog3*$^{TA.pUD}$ cells (Fig. 2C,D). These data, along with the knowledge that nearly all (~96%) *Neurog3*-based lineage-labeled cells ultimately adopt the endocrine lineage (Schonhoff et al. 2004; Zhang et al. 2009), indicate that the Sox9$^+$ *Neurog3*$^{TA.pUD}$ and Sox9$^+$ *Neurog3*$^{TA.pLO}$ populations together—collectively referred to here as the Sox9$^+$ *Neurog3*$^{TA.LO}$ population (Supplemental Table S1)—represent a mitotic endocrine-biased progenitor pool. The evidence from pHH3$^+$ quantification is strengthened below in real-time tracing of this population with a new *Neurog3* reporter. In addition, comparing Sox9$^+$ *Neurog3*$^{TA.LO}$ progenitor numbers relative to Sox9$^-$ lineage-labeled *Neurog3*^{pHI} (referred to here as *Neurog3*$^{TA.HI}$) endocrine-committed cells revealed a shift toward *Neurog3*$^{TA.HI}$ cells at E14.5 versus E12.5 (Supplemental Fig. S4), the same pattern as seen in Figure 1D. In sum, we propose that tracking *Neurog3* transcriptional activity marks the true intraepithelial *Neurog3*^{LO} mitotic progenitor state that is responsible for deriving endocrine-committed Neurog3^{HI} cells.

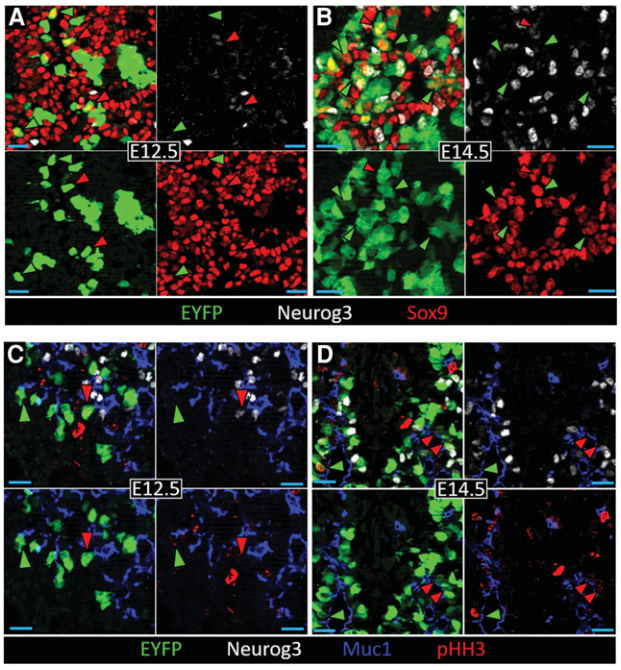

Figure 2. *Neurog3*^{TA} Sox9$^+$ cells, comprising *Neurog3*$^{TA.pLO}$ and *Neurog3*$^{TA.pUD}$ cells, represent a mitotic *Neurog3*$^{TA.LO}$ endocrine-biased progenitor pool. E12.5 (*A*,*C*) and E14.5 (*B*,*D*) pancreatic epithelium showing EYFP, Neurog3, and Sox9 or EYFP, Neurog3, Muc1, and pHH3. (*A*,*B*) Red and green arrowheads indicate Sox9$^+$ EYFP$^+$ *Neurog3*$^{TA.pLO}$ cells and Sox9$^+$ EYFP$^+$ *Neurog3*$^{TA.pUD}$ cells, respectively. (*C*,*D*) Red and green arrowheads indicate pHH3$^+$ Muc1$^+$ *Neurog3*$^{TA.pLO}$ and pHH3$^+$ Muc1$^+$ *Neurog3*$^{TA.pUD}$ cells, respectively.

Tracking mitotic Neurog3$^{TA.LO}$ *progenitors via a novel* Neurog3 *BAC transgenic reporter*

Although the indelible marking of *Neurog3*-expressing cells by the *Neurog3*$^{BAC.Cre}$;*R26R*^{EYFP} system is useful for lineage tracing studies, the cumulative nature of this labeling system potentially loses critical aspects of dynamic gene expression. We therefore generated a new, sensitive *Neurog3*-driven H2B^{mCherry}-peptide-2A-GFP^{GPI} BAC transgenic reporter mouse (*Neurog3*^{RG1}) that uses a peptide 2A breaker for simultaneous marking of the chromatin (histone H2B^{mCherry} fusion ["R"]) and plasma membrane (glycosylphosphatidylinositol [GPI]-EGFP fusion ["G"]) of *Neurog3*-expressing cells (Supplemental Fig. S5A). The design of the *Neurog3*^{RG1} reporter as a BAC transgenic followed several criteria outlined in the Supplemental Material and avoided any negative impact on progenitor behavior caused by engineering the native *Neurog3* locus (Wang et al. 2010). Examination of gross tissue morphology and scoring cell type proportional representations—especially focusing on nascent and hormone-expressing endocrine cells over various phases of pancreatogenesis—revealed no abnormal phenotype in *Neurog3*^{RG1} reporter mice (Supplemental Fig. S5B–E). Glucose levels of ad libitum fed *Neurog3*^{RG1} mice were similar to wild-type littermates (Supplemental Table S2). The numbers of Sox9$^+$ Neurog3^{pLO} cells and Sox9$^-$ Neurog3^{pHI} cells at E12.5 and E14.5 were also unchanged in *Neurog3*^{RG1} transgenic mice relative to wild type (Supplemental Table S2). Rigorous quantification revealed that the majority of Neurog3$^{Protein+}$ cells (low and high Neurog3$^+$ cells together) coexpressed the *Neurog3*^{RG1} reporter (60% ± 3.2% at E12.5 and 70% ± 7.7% at E14.5) (Supplemental Table S2). Although all *Neurog3*$^{RG1+}$ Neurog3^{pHI} cells showed both mCherry and EGFP signals, the more rapid maturation time of mCherry (~15 min) (Shaner et al. 2005) caused a portion of intraepithelial *Neurog3*$^{RG1+}$ Neurog3^{pLO} cells to be only mCherry$^+$ (Supplemental Fig. S5B–D); we presume that these cells would later have become red/green dual-fluorescent. *Neurog3* expression normally decreases following hormone expression, but the H2B^{mCherry} longevity and, to a much lesser extent, GFP^{GPI} caused red/green labeling in some hormone-expressing endocrine cells and an enduring red signal in cells contained within islet clusters (Supplemental Fig. S5D,E). Similar to earlier findings (Fig. 2), at both E12.5 and E14.5, *Neurog3*^{RG1} transcription reporting

marked Sox9^{+} *Neurog3*^{pUD} as well as *Neurog3*^{pLO} cells (Figs. 3A,B, 6A), with a significant number of the overall *Neurog3*$^{TA.LO}$ population being pHH3^{+} (Fig. 3C,D). Additionally, the number of Sox9^{+} *Neurog3*$^{RG1+}$ *Neurog3*$^{TA.LO}$ cells relative to Sox9^{-} *Neurog3*$^{RG1+}$ *Neurog3*$^{TA.HI}$ cells showed a shift in favor of endocrine commitment at E14.5 versus E12.5 (Fig. 3E), similar to the *Neurog3*^{Cre}-based lineage tracing result (Supplemental Fig. S4). The higher proportion of Sox9^{+} *Neurog3*$^{TA.LO}$ cells relative to Sox9^{-} *Neurog3*$^{TA.HI}$ cells (Supplemental Fig. S4 vs. Fig. 3E) likely represents the cumulative labeling over a substantial time period within which Cre activates the binary *R26R* reporter, whereas the "snapshot" analysis via the *Neurog3*^{RG1} reporter might detect only a subset in which the fluorescence is detectable at the time of analysis. These data validate the *Neurog3*^{RG1} mouse line as a passive reporter that correctly marks the various states of *Neurog3* expression in the intraepithelial and delaminated stages of endocrine ontogeny.

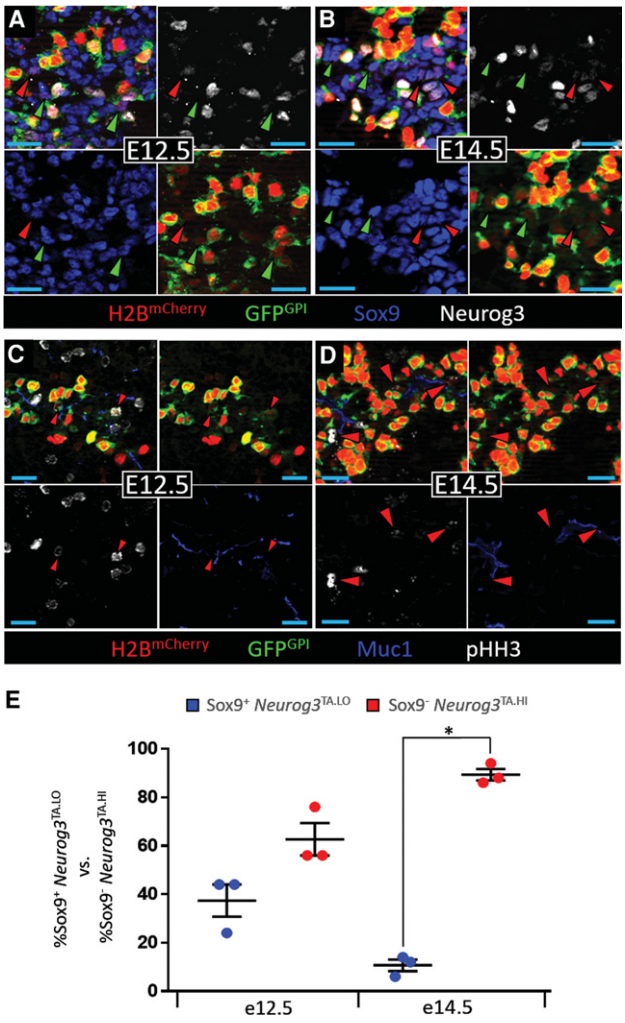

Figure 3. The *Neurog3*^{RG1} transgenic reporter marks the mitotic *Neurog3*$^{TA.LO}$ progenitor population. E12.5 (*A*,*C*) and E14.5 (*B*,*D*) pancreatic epithelium showing H2B^{mCherry}, GFP^{GPI}, Sox9, and Neurog3 or H2B^{mCherry}, GFP^{GPI}, Muc1, and pHH3. (*A*,*B*) Red and green arrowheads indicate Sox9^{+} *Neurog3*$^{TA.pLO}$ and Sox9^{+} *Neurog3*$^{TA.pUD}$ cells (seen by low H2B^{mCherry} signal from *Neurog3*^{RG1}), respectively. (*C*,*D*) Red arrowheads indicate Muc1^{+} *Neurog3*$^{RG1+}$ pHH3^{+} *Neurog3*$^{TA.LO}$ cells. (*E*) The percentage of *Neurog3*$^{RG1+}$ Sox9^{+} *Neurog3*$^{TA.LO}$ versus *Neurog3*$^{RG1+}$ Sox9^{-} *Neurog3*$^{TA.HI}$ cells at E12.5 ($n = 585$; $N = 3$) and E14.5 ($n = 6334$; $N = 3$). Data are mean ± SEM. (*) $P = 1 \times 10^{5}$.

Comparison of Neurog3$^{TA.LO}$ *progenitors with endocrine-committed cells captured via* Neurog3^{RG1} *reporting*

The *Neurog3*^{RG1} reporter was immediately valuable in revealing, at relatively high resolution, not only the behavior of intraepithelial *Neurog3*$^{TA.LO}$ progenitors by time-lapse imaging but also the derivation and delamination of endocrine-committed *Neurog3*$^{TA.HI}$ cells. During an initial analysis, we observed a previously unknown feature of delaminating *Neurog3*$^{TA.HI}$ cells (Supplemental Fig. S6A). Specifically, *Neurog3*$^{TA.HI}$ cells entering delamination showed an early apical membrane narrowing, but later, when most of the cell body had become displaced from the main epithelial layer, there was a pervasive narrow tether-like connection to an almost punctate apical contact at the lumen (Supplemental Fig. S6). Time-lapse imaging of E14.5 *Neurog3*$^{RG1+}$ explants showed that the process of delamination, from initial apical narrowing of a *Neurog3*$^{TA.HI}$ cell to its epithelial detachment, lasted upward of 16 h, with a majority of this period spent in the tethered state (Supplemental Fig. S6B,D; Supplemental Movie 1). Quantification of delaminating *Neurog3*$^{RG1-HI}$ cells showed that 100% involved apically connected lumenal tethers (CVE Wright, ME Bechard, and E Bankaitis, in prep.; data not shown). The prolonged lumenal contact during delamination of *Neurog3*$^{TA.HI}$ cells means that both they and Sox9^{+} *Neurog3*$^{TA.LO}$ cells were Muc1^{+} (Supplemental Fig. S6C). Combining Muc1 positivity with *Neurog3*^{RG1} reporter expression thus provided an opportunity to flow-sort and separate intraepithelial progenitors (Muc1^{+} *Neurog3*$^{RG1-LO}$) (Supplemental Table S1) and actively delaminating cells (Muc1^{+} *Neurog3*$^{RG1-HI}$) (Supplemental Table S1) to characterize their progenitor–precursor relationship. To accomplish this, *Neurog3*$^{RG1+}$ E12.5 and E14.5 explants were flow-sorted first for Muc1 positivity and then according to low or high *Neurog3*^{RG1} fluorescence (Supplemental Fig. S7A). Analysis via quantitative RT–PCR (qRT–PCR) showed that sorted *Neurog3*$^{RG1-HI}$ cells from E12.5 and E14.5 pancreata, in addition to negligible *Sox9* expression, were highly enriched for *Neurog3*, *glucagon*, *insulin* (but in E14.5 samples only), *Pax6*, and *NeuroD1* (Supplemental Figs. S7B, S8). *Neurog3*$^{RG1-HI}$ cells were highly enriched for *Cdkn1a* (Supplemental Fig. S8), which promotes cell cycle exit and is a known target of *Neurog3* (Miyatsuka et al. 2011). Recently, *Hnf1b* was shown to be a critical positive regulator of *Neurog3* expression (De Vas et al. 2015). Our analysis, however, shows higher *Hnf1b* expression in *Neurog3*$^{TA.HI}$ cells versus *Neurog3*$^{TA.LO}$ cells (Supplemental Fig. S8), which could indicate a role in activating *Neurog3* expression

during the early *Neurog3*$^{TA.LO}$-to-*Neurog3*$^{TA.HI}$ transition. These data are consistent with actively delaminating Muc1^{+} *Neurog3*$^{RG1\text{-}HI}$ cells being post-mitotic, undergoing endocrine commitment toward the hormone-expressing condition. In contrast, sorted *Neurog3*$^{RG1\text{-}LO}$ cells had significantly lower *Neurog3* expression and negligible *glucagon*, *Pax6*, or *NeuroD1* expression, with significant enrichment in *Sox9*, *Hes1*, and *Hnf6* (Supplemental Figs. S7B, S8). Consistent with their mitotic nature, *cyclin-dependent kinase 6* (*Cdk6*; a positive cell cycle regulator) was enriched in *Neurog3*$^{RG1\text{-}LO}$ cells (Supplemental Fig. S8). Because *Sox9*, *Hes1*, and *Hnf6* are accepted progenitor-state markers within the bipotent population of the trunk epithelium, these data fit with the Sox9^{+} *Neurog3*$^{TA.LO}$ population being at or close to a progenitor state.

Real-time analysis of mitotic Neurog3$^{TA.LO}$ *cells*

To investigate further our proposal that Sox9^{+} *Neurog3*$^{TA.LO}$ cells give rise to both *Neurog3*$^{TA.LO}$ progenitors and endocrine-committing post-mitotic *Neurog3*$^{TA.HI}$ precursors, E12.5 *Neurog3*^{RG1} explants were subjected to time-lapse imaging focusing on intraepithelial low-level fluorescing cells. Dividing *Neurog3*$^{TA.LO}$ cells and their progeny were followed for ~12–24 h (Supplemental Table S3); imaging was restricted to ~24 h because the end of this period started to show presumably phototoxic effects on tissue growth and cell survival, a known consequence of confocal laser exposure (Stephens and Allan 2003). The size of the pancreatic explants (~50–100 µm thick) and substantial light scattering in deep-tissue imaging served to limit our analysis to ~30 µm closest to the microscope objective (Supplemental Table S3). Within this depth, we observed an average of three intraepithelial *Neurog3*$^{RG1\text{-}LO}$ mitotic events per explant—a total of 15 over five real-time imaging runs (Supplemental Table S3). Although an apical marker was absent during our real-time analysis, a *Neurog3*$^{TA.LO}$ cell was assigned as intraepithelial by the extent of its apical surface, the lack of the narrow tether seen on delaminating *Neurog3*$^{RG1\text{-}HI}$ cells, and nuclear proximity to the lumen (Fig. 4A,B). Several factors likely contributed to observing what is probably a subset of the true number of Sox9^{+} *Neurog3*$^{TA.LO}$ cell divisions occurring within the pancreatic epithelium in vivo. First, the relatively high number of *Neurog3*$^{RG1+}$ cells and high fluorescence in *Neurog3*$^{RG1\text{-}HI}$ cells in the E12.5–E13.5 period meant that divisions were clearly discernible only in regions less densely populated by *Neurog3*$^{RG1+}$ cells. Second, the pancreatic epithelium is approximately fourfold less mitotically active under ex vivo culture conditions (Puri and Hebrok 2007; Kim et al. 2015). To determine whether the observed division events produced *Neurog3*$^{TA.LO}$ cells or *Neurog3*$^{TA.HI}$ cells, the level of H2B^{mCherry} fluorescence intensity in the nucleus of an intraepithelial *Neurog3*$^{RG1\text{-}LO}$ cell was quantified first at the initial appearance of mitotic chromosomes (Supplemental Table S3). Although details of H2B^{mCherry} fluorescence are reported for this analysis, the GFP^{GPI} fluorescence intensity provided matching information. Next, the fluorescence intensity of *Neurog3*^{RG1}-expressing daughters was quantified ~3–6 h after division, with fluorescence intensity quantification beyond 6 h being dependent on how long the daughter cells were tracked before video termination or whether they moved out of view (Supplemental Table S3). *Neurog3*$^{RG1+}$ daughter cells were determined to have initiated delamination if they increased the *Neurog3*^{RG1} fluorescence intensity or showed basal-ward displacement of their nucleus/cell body or other signs of delamination, such as basally directed membrane-protrusive behavior, formation of the lumenal tether, and greatly narrowed apical contact. By these parameters, two division categories were observed. In the first, a *Neurog3*$^{RG1\text{-}LO}$ cell produced two daughters, each increasing *Neurog3*^{RG1} reporter fluorescence intensity by an average of ~2.5-fold and simultaneously exhibiting signs of delamination (Fig. 4A; Supplemental Table S3; Supplemental Movie 2). This division was a symmetric division terminal differentiation event in which both

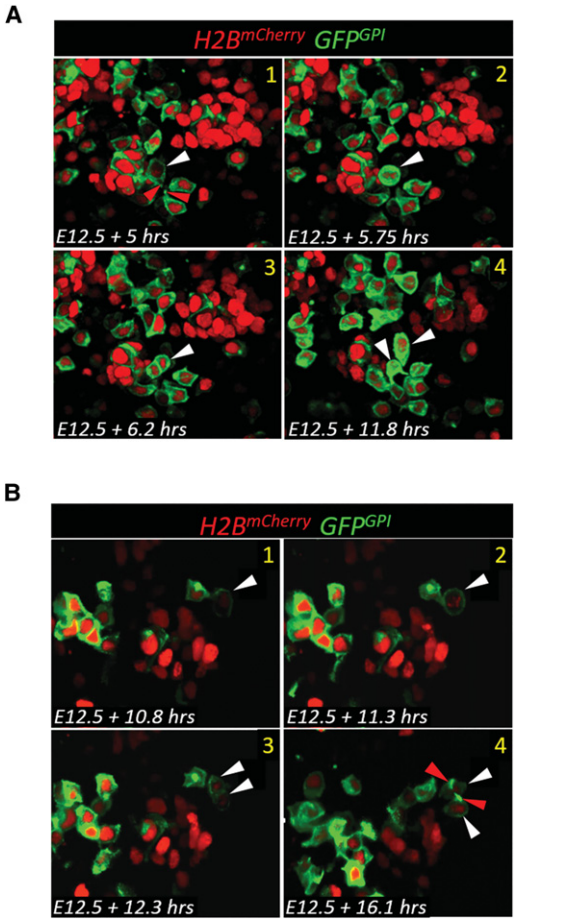

Figure 4. Division of *Neurog3*$^{TA.LO}$ progenitors in real time. Division of a *Neurog3*$^{TA.LO}$ cell into two delaminating *Neurog3*$^{TA.HI}$ cells (*A*) or two *Neurog3*$^{TA.LO}$ progenitors (*B*). Images are screen captures from Fig. 4B; Supplemental Movie 2. White and red arrowheads indicate a *Neurog3*$^{TA.LO}$ division event and apical attachment, respectively.

daughters moved toward endocrine commitment, with the transition from *Neurog3*$^{TA.LO}$ to *Neurog3*$^{TA.HI}$ (as marked by the *Neurog3*^{RG1} reporter) taking ~3–6 h. In the second type of division, a *Neurog3*$^{RG1\text{-}LO}$ cell produced two daughters that did not increase *Neurog3*^{RG1} reporter fluorescence intensity, exhibited no filopodial exploratory behavior at the basal surface or other signs of delamination, and remained in an intraepithelial location (Fig. 4B; Supplemental Table S3; Fig. 4B; Supplemental Movie 3). This type of division was classified as symmetric division progenitor maintenance: a *Neurog3*$^{TA.LO}$ progenitor producing daughters that both remained in the *Neurog3*$^{TA.LO}$ progenitor state. Intraepithelial Sox9^{+} *Neurog3*$^{TA.LO}$ progenitors are thus able to undergo divisions that either produce more progenitors or give rise to more differentiated progeny. Of the observable mitotic events scorable during these movies, all occurred in *Neurog3*$^{TA.LO}$ (*Neurog3*$^{RG\text{-}LO}$) cells; no *Neurog3*$^{RG\text{-}HI}$ divisions were observed. There was an overall 53%:47% split between progenitor maintenance and symmetric terminal differentiation divisions, and no asymmetric cell divisions were observed, forming one *Neurog3*$^{TA.LO}$ and one *Neurog3*$^{TA.HI}$ cell. We consider these data to be in accordance with the incipient building up of the endocrine-biased progenitor pool during the rapid plexus expansion occurring at this stage of pancreas organogenesis.

Although not directly observed in our time-lapse movies (possibly because of the restricted time-lapse period and the slowing of mitotic activity ex vivo), we hypothesized that mitotic *Neurog3*$^{TA.LO}$ progenitors in vivo can undertake multiple rounds of division to produce, over time, considerable numbers of *Neurog3*$^{TA.LO}$ progenitors or *Neurog3*$^{TA.HI}$ cells. Sequential dual-thymidine analog labeling is one way of tracking cells that divide more than once (Teta et al. 2007; Bradford and Clarke 2011). To determine the relative rate at which multiple rounds of progenitor maintenance versus terminal differentiation occurred, we quantified the relative proportion of EdU/BrdU double-labeled *Neurog3*^{pLO} cells versus EdU/BrdU double-labeled *Neurog3*^{pHI} cells. To accomplish this, E12.5 or E14.5 pancreatic epithelium was labeled sequentially with single EdU and BrdU injections 12 h apart (Supplemental Fig. S9A). To avoid fluorescence crossover problems when combining mCherry/GFP signals from *Neurog3*^{RG1} with EdU/BrdU immunofluorescence signals, we used Neurog3 protein to define *Neurog3*$^{TA.LO}$ and *Neurog3*$^{TA.HI}$ cells. Despite the likely underscoring of *Neurog3*$^{TA.LO}$ cells by using this method (for reasons described above), we show that the percentage of EdU^{+}BrdU^{+} Neurog3^{pLO} cells is ~3.2-fold higher than that of EdU^{+}BrdU^{+} Neurog3^{pHI} cells at E12.5, compared with equal proportions of the two populations at E14.5 under the same labeling scheme (Supplemental Fig. S9B,D, E). It is possible that the complex plexus-state epithelium in vivo displays spatiotemporally varied behavior of *Neurog3*$^{TA.LO}$ progenitors with respect to their frequency of undergoing multiple rounds of division. Our snapshot-style bulk analysis will therefore tend toward a "homogenizing" nature when scoring across such a largely asynchronous epithelium and underrepresent the variation in mitotic activity of *Neurog3*$^{TA.LO}$ progenitors as the plexus-state endocrine progenitor niche develops, moves toward a state of peak endocrine yield, and begins final remodeling to the mature ductal tree. Nevertheless, these data fit the notion that, early in the secondary transition, progenitor maintenance-type division of the Sox9^{+} *Neurog3*$^{TA.LO}$ pool is favored over symmetric terminal differentiation-type division (Supplemental Fig. S9C). As the pancreatic epithelium progresses through the secondary transition, however, the proportion of terminal differentiation events could increase to accommodate local increases in endocrine cell birth rate.

Limiting Neurog3 *expression increases proliferation and expands the* Neurog3$^{TA.LO}$ *progenitor pool*

We tested whether deliberately reducing the level of *Neurog3* gene activity would increase the proliferative index of *Neurog3*$^{TA.LO}$ progenitors and/or cause a concomitant population expansion. We determined the number and mitotic activity of Sox9^{+} *Neurog3*$^{TA.LO}$ cells in a decreasing series of gene dosages: wild-type, *Neurog3* heterozygous (*Neurog3*$^{EGFP/+}$), and strong *Neurog3* hypomorphic (*Neurog3*$^{EGFP/FL}$) conditions. At E14.5, *Neurog3* expression and protein levels in the developing pancreas are known to decrease by ~50% in the heterozygous condition and ~75% under the strong hypomorphic condition (Wang et al. 2010) and are known to release *Neurog3*-expressing cells to nonendocrine lineages in both "reduced dosage" states. In that study, a large increase in *Neurog3*-expressing epithelial cells occurred in the strong hypomorphic condition compared with the heterozygous condition (Wang et al. 2010). However, the *Neurog3*^{EGFP} reporter that they used was *Neurog3*-null, preventing comparison with wild-type tissues. Our new *Neurog3*^{RG1} reporter does not perturb the endogenous locus and thus allows this comparison. We reasoned that the *Neurog3*^{RG1} BAC transgene reporter (see the Supplemental Material) would behave similarly to the endogenous locus EGFP knock-in for estimating dynamic behavior of the *Neurog3*$^{TA.LO}$ population. We decided against using *Neurog3*$^{BAC.Cre}$;*R26R*^{EYFP} lineage tracing in the wild-type condition, which captures the population cumulatively via a dual-gene activation system. In areas of plexus-like epithelium that are rich in endocrine-committing and delaminating Neurog3^{HI} cells, the visual estimation of the prevalence of the intraepithelial *Neurog3*$^{TA.LO}$ population was similar for *Neurog3*^{RG1} (Fig. 3A,B) and *Neurog3*$^{EGFP/+}$ tissue (Fig. 5A,B), which was then validated by quantification across the epithelium (Fig. 6C), supporting the idea that both are effective for probing the population behavior of the *Neurog3*$^{TA.LO}$ pool. In all three genotypes—wild type (containing *Neurog3*$^{RG1+}$), heterozygous *Neurog3*$^{EGFP/+}$, and strong hypomorphic *Neurog3*$^{EGFP/FL}$—we could easily observe *Neurog3*$^{TA.pLO}$ (Neurog3 protein-low) and *Neurog3*$^{TA.pUD}$ (Neurog3 protein-undetectable) cells. As for the wild-type tissue, the heterozygous and the strong hypomorph conditions also showed significant numbers of their overall EGFP^{+} Sox9^{+} *Neurog3*$^{TA.LO}$ population as pHH3^{+} (Fig. 5E–H). Quantification

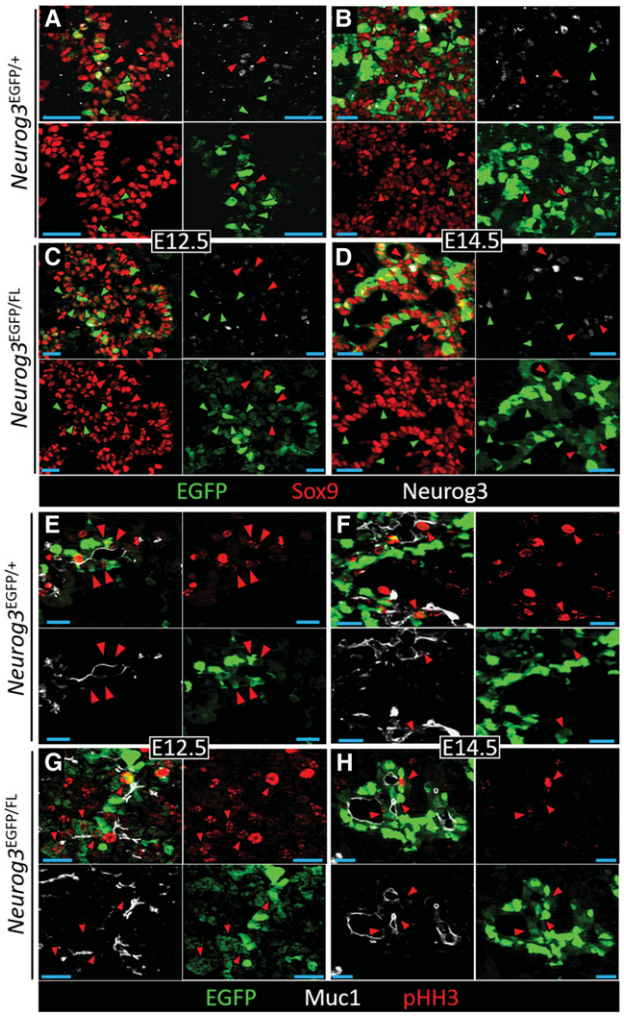

Figure 5. The mitotic *Neurog3*$^{TA.LO}$ population is prevalent under *Neurog3* heterozygous and strong hypomorphic conditions. E12.5 (*A*,*C*,*E*,*G*) and E14.5 (*B*,*D*,*F*,*H*) pancreatic epithelium showing EGFP, Neurog3, and Sox9 or EGFP, Muc1, and pHH3 from *Neurog3*$^{EGFP/+}$ and *Neurog3*$^{EGFP/FL}$ embryos. (*A–D*) Red and green arrowheads indicate Sox9$^+$ *Neurog3*$^{TA.pLO}$ and Sox9$^+$ *Neurog3*$^{TA.pUD}$ cells (marked by low EGFP signal from *Neurog3*^{EGFP}), respectively. (*E–H*) Red arrowheads indicate Muc1$^+$ EGFP$^+$ pHH3$^+$ *Neurog3*$^{TA.LO}$ cells.

showed that, relative to the wild type, the number of Sox9$^+$ *Neurog3*$^{TA.pUD}$ cells was significantly (and equivalently) greater than Sox9$^+$ *Neurog3*$^{TA.pLO}$ cells under *Neurog3* heterozygous and strong hypomorphic conditions at both E12.5 and E14.5 (Figs. 5C,D, 6A). We also observed, at E12.5, a significantly increased Sox9$^+$ *Neurog3*$^{TA.LO}$ progenitor pool (combining protein-low and protein-undetectable cells) relative to the endocrine-committed *Neurog3*$^{TA.HI}$ pool in the heterozygous and strong hypomorphic conditions (cf. Figs. 3E and 6B). As described above (Figs. 1D, 3E), wild-type tissue showed a significantly increased *Neurog3*$^{TA.HI}$ relative to *Neurog3*$^{TA.LO}$ cell number between E12.5 and E14.5. The degree of this temporal shift toward the *Neurog3*$^{TA.HI}$ pool was much reduced in the heterozygous condition and nearly absent in the strong hypomorph (Figs. 3E vs. 6B). These results suggest that limiting *Neurog3* expression—and thus protein levels—increased the number of Sox9$^+$ *Neurog3*$^{TA.LO}$ progenitors undergoing progenitor maintenance divisions relative to terminal differentiation-type divisions.

We next determined whether the increased production of Sox9$^+$ *Neurog3*$^{TA.LO}$ progenitors under reduced gene dosage affected the overall proportional representation of the intraepithelial *Neurog3*$^{TA.LO}$ progenitor population. Compared with the wild-type (*Neurog3*$^{RG1+}$) control, the proportion of Sox9$^+$ *Neurog3*$^{TA.LO}$ cells under the heterozygous condition, although unchanged at E12.5, was 2.5-fold expanded at E14.5 (Fig. 6C). Under the strong hypomorphic condition, however, this population was increased eightfold at E12.5 and 14-fold at E14.5 (Fig. 6C). These expansions were associated with increased proliferation as marked by pHH3. As explained above (Fig. 2), only *Neurog3*^{TA} cells (*Neurog3*^{RG1}-positive cells) with clear Muc1$^+$ surfaces were defined as intraepithelial and with DAPI as an aid where appropriate. The mitotic index of *Neurog3*$^{TA.LO}$ cells in *Neurog3*$^{EGFP/+}$ heterozygous relative to the wild type, although unchanged at E12.5, was increased 1.4-fold at E14.5 (Fig. 7A). In the *Neurog3*$^{EGFP/FL}$ strong hypomorph, however, the index was increased 2.1-fold at E12.5 and 1.7-fold at E14.5 (Fig. 7A). We also scored for any non-cell-autonomous effect of limiting *Neurog3* expression on the mitotic index of the surrounding *Neurog3*-nonexpressing (Muc1$^+$ *Neurog3*$^-$) epithelium but found no significant change (Fig. 7A). These findings are consistent with a low level of Neurog3 protein having a critical role in the maintenance of an actively cycling, endocrine-biased *Neurog3*$^{TA.LO}$ progenitor state (Fig. 7B).

Discussion

We describe several lines of evidence pointing to a new model for the generation of endocrine-committed Neurog3^{HI} cells during the pancreatic secondary transition, driven by an intraepithelial endocrine-biased mitotic *Neurog3*$^{TA.LO}$ progenitor population (Fig. 7B). Using *Neurog3*-driven transcriptional reporters, we show that these progenitors are relatively abundant and have prolonged residency within the plexus-state epithelium of the developing pancreas, undertaking symmetric divisions to maintain the progenitor pool or produce two endocrine-committing daughters. As a mitotic pool that continually feeds production of endocrine-committed cells by symmetric terminal differentiation division, its behavior is reminiscent of progenitors in other tissues (for example, the intestinal crypt), acting as a transit-amplifying population. We do not propose that the *Neurog3*$^{TA.LO}$ progenitor pool is set aside at a very early stage of pancreas development, within the primary transition. However, further investigation (probably requiring lineage tracing tools capable of labeling only *Neurog3* low-level expressors) would be needed to distinguish whether the Sox9$^+$ *Neurog3*$^{TA.LO}$ endocrine-biased progenitor pool continues to

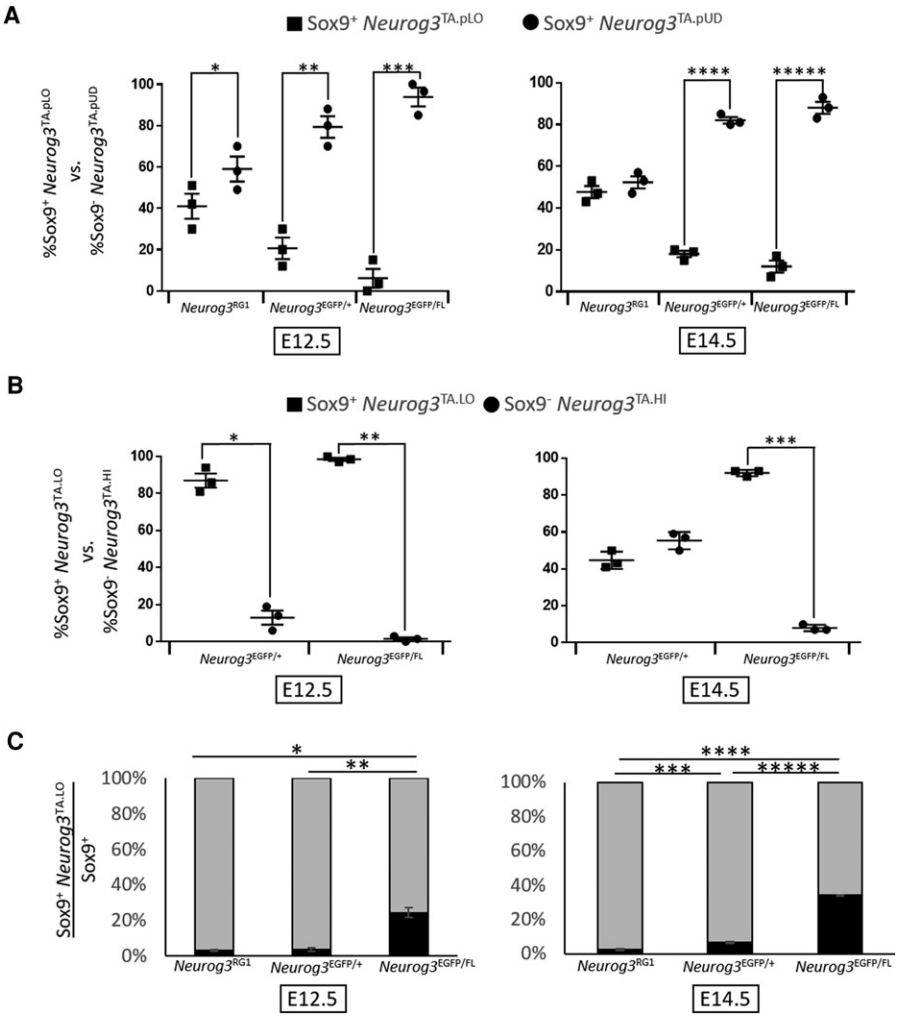

Figure 6. Limiting *Neurog3* expression expands the *Neurog3*$^{TA.LO}$ population at the expense of *Neurog3*$^{TA.HI}$ cells. (*A*) The percentage of Sox9$^+$ *Neurog3*$^{TA.pLO}$ versus Sox9$^+$ *Neurog3*$^{TA.pUD}$ cells in wild-type (*Neurog3*^{RG1}) (see Fig. 3E for *n*), *Neurog3*$^{EGFP/+}$ (E12.5, $n = 168$, $N = 3$; E14.5, $n = 2425$, $N = 3$), and *Neurog3*$^{EGFP/FL}$ (E12.5, $n = 1237$, $N = 3$; E14.5, $n = 5818$, $N = 3$) pancreata. (*) $P = 0.0523$; (**) $P = 0.00067$; (***) $P = 8.3 \times 10^{-5}$; (****) $P = 4 \times 10^{-6}$; (*****) $P = 2.5 \times 10^{-5}$. (*B*) The percentage of Sox9$^+$ *Neurog3*$^{TA.LO}$ versus Sox9$^-$ *Neurog3*$^{TA.HI}$ cells in *Neurog3*$^{EGFP/+}$ and *Neurog3*$^{EGFP/FL}$ (see *A* for *n*) pancreata. (*) $P = 8 \times 10^{-5}$; (**) $P = 8 \times 10^{-8}$; (***) $P = 2.4 \times 10^{-7}$. (C) The percentage of Sox9$^+$ cells that are *Neurog3*$^{TA.LO}$ in wild-type (*Neurog3*^{RG1}) (E12.5, $n = 4497$, $N = 3$; E14.5, $n = 11930$, $N = 4$), *Neurog3*$^{EGFP/+}$ (E12.5, $n = 4718$; E14.5, $n = 15903$), and *Neurog3*$^{EGFP/FL}$ (E12.5, $n = 4656$; E14.5, $n = 15671$) pancreata. (*) $P = 0.00015$; (**) $P = 0.0009$; (***) $P = 0.0022$; (****) $P = 2 \times 10^{-7}$; (*****) $P = 1 \times 10^{-6}$. Data are mean ± SEM.

be established throughout the secondary transition by derivation from a parental bipotent (duct/endocrine) trunk epithelium population or is essentially completely allocated within a short period near the inception of the secondary transition. If the latter result were to be found, it would support one interpretation of a previous lineage tracing study (Gu et al. 2002) showing that a large-scale separation of the duct and endocrine progenitors occurs in the run-up to the secondary transition as the plexus-state trunk epithelium becomes organized. The intraepithelial *Neurog3*$^{TA.LO}$ pool is likely maximally estimated through the use of *Neurog3*$^{BAC.Cre}$;*R26R*^{EYFP} lineage labeling, in which we determined that, at E14.5, about one-quarter of the whole Sox9$^+$ epithelium was in the *Neurog3*$^{TA.LO}$ state. These cells were often clustered together, not scattered homogeneously, and scoring specifically plexus-state epithelial cells revealed up to half of them in this state. Our snapshot-type longitudinal analysis leaves open the possibility that any individual area of the plexus might have juvenile, mature, and aged phases in which the proportional representation of *Neurog3*$^{TA.LO}$ cells varies (according to developmental inputs), with all regions at some time passing through a "peak occupancy" period. Regarding our finding that reducing *Neurog3* expression led to expansion of the Sox9$^+$ *Neurog3*$^{TA.LO}$ progenitor population and significantly increased its mitotic index, these effects on the *Neurog3*$^{TA.LO}$ pool may also be underestimated by our scoring large regions of epithelium without being able to refer to spatial variations in the relative maturity of individual epithelial regions.

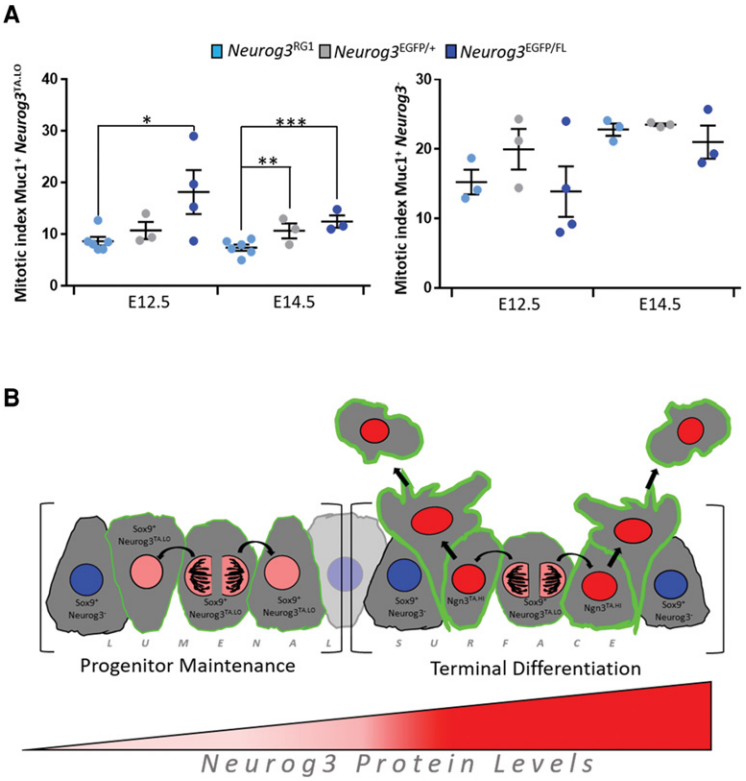

Figure 7. Reducing *Neurog3* expression increases the mitotic index of Sox9$^+$ *Neurog3*$^{TA.LO}$ progenitors. (*A*, *left*) The mitotic index (percentage pHH3$^+$) of Muc1$^+$ *Neurog3*$^{TA.LO}$ cells under wild-type (*Neurog3*^{RG1}) (E12.5, $n = 569$, $N = 6$; E14.5, $n = 2401$, $N = 6$), *Neurog3*$^{EGFP/+}$ (E12.5, $n = 362$, $N = 3$; E14.5, $n = 904$, $N = 3$), and *Neurog3*$^{EGFP/FL}$ (E12.5, $n = 783$, $N = 4$; E14.5, $n = 3905$, $N = 3$) conditions. (*Right*) The mitotic index of Muc1$^+$ *Neurog3*$^-$ cells in wild-type (*Neurog3*^{RG1}) (E12.5, $n = 1200$ cells, $N = 3$; E14.5, $n = 7490$, $N = 3$), *Neurog3*$^{EGFP/+}$ (E12.5, $n = 1003$, $N = 3$; E14.5, $n = 2737$, $N = 3$) and *Neurog3*$^{EGFP/FL}$ (E12.5, $n = 2226$, $N = 4$; E14.5, $n = 5217$, $N = 3$) pancreata. Data are mean ± SEM. (*) $P = 0.0138$; (**) $P = 0.0207$; (***) $P = 0.0018$. (*B*) Model depicting the behavior of *Neurog3*$^{TA.LO}$ cells in the pancreatic epithelium.

Our findings fit better with aspects of *Neurog3* expression data reported in previous literature that were not previously highlighted, providing a new level of clarity regarding the role of *Neurog3* in directing endocrine cell production during the secondary transition. Below, we speculate that our findings may indicate an interesting parallel with the role of the Neurog3 sister protein Neurog2 in neuronal development. Taking into account that the final endocrine cell fate choice is thought to have occurred in *Neurog3*-expressing cells (Desgraz and Herrera 2009), future experiments should investigate whether lineage specification/commitment might occur in the *Neurog3*$^{TA.LO}$ endocrine-biased progenitor state. Such information could advance efforts to manipulate human pluripotent stem cell-derived endocrine progenitors into producing specific types and quantities of functional endocrine cells.

Low Neurog3 *expression defines an endocrine-biased mitotic progenitor state in Sox9$^+$ cells*

Our conclusion that Sox9$^+$ *Neurog3*$^{TA.LO}$ progenitors represent an actively cycling, discrete, endocrine-biased progenitor population is consistent with previous in situ hybridizations using probe cocktails marking early steps of endocrine ontogeny to show broad mRNA distributions across most of the E14.5 epithelium (Zhou et al. 2007). These data corroborate the notion that many intraepithelial cells have entered the endocrine lineage program, maybe even in a relatively concerted manner beyond activating only *Neurog3* expression (Zhou et al. 2007). *Neurog3*$^{BAC.Cre}$-based lineage tracing in wild-type tissue shows that almost all *Neurog3*$^+$ cells move eventually into the endocrine lineage, with a small percentage adopting nonendocrine acinar or duct lineages (Schonhoff et al. 2004). Furthermore, reducing *Neurog3* expression via heterozygous/hypomorphic alleles significantly decreases the degree of endocrine biasing, allowing increased drift to nonendocrine lineages (Wang et al. 2010). Fitting our results with these studies prompts the conclusion that normal *Neurog3*$^{TA.LO}$ cells represent an endocrine-biased progenitor state that retains a small degree of multipotency. It will be interesting to determine, perhaps via single-cell RNA sequencing analysis, whether a low-level "sampling" type of expression activates, in *Neurog3*$^{TA.LO}$ endocrine-biased progenitors, genes lying downstream in the endocrine lineage specification–commitment–differentiation program, such as *Insm1A*, *Pax4*, *Nkx2.2*, and *Arx*. The notion that *Neurog3*$^{TA.LO}$ progenitors are noncommitted but nonetheless access endocrine pathway programs targeted by Neurog3 is analogous to the concept that, during hematopoiesis, progenitor cells are selectively primed toward multiple lineage programs (Nimmo et al. 2015).

Our confirmation that almost all *Neurog3*$^{TA.HI}$ cells are post-mitotic fits with previous studies demonstrating that high Neurog3 protein levels instruct cell cycle exit and transition to a unipotent precursor state producing an individual endocrine cell type (Desgraz and Herrera 2009). We propose that those previous studies focused on endocrine-committed Neurog3^{HI} cells, not low-level epithelial *Neurog3*$^{TA.LO}$ cells, because certain lineage tracer

Neurog3^{Cre} driver/reporter pairings (for example, the *Neurog3*^{Cre};Z/AP reporter system) (Gu et al. 2002) require a higher level of *Neurog3*^{Cre} expression that is reached only during endocrine commitment, thus missing the low-level-expressing intraepithelial cells. It is plausible that the increased ability of the *Neurog3*$^{BAC.Cre}$ (Schonhoff et al. 2004) to switch on *R26R*-based lineage reporters relates to *cis*-regulatory regions present in the BAC transgene that augment the known enhancer promoter elements of *Neurog3* (Lee et al. 2001; Ejarque et al. 2013). Likely, our selection of the same *Neurog3* BAC used by Schonhoff et al. (2004) in our *Neurog3*^{RG1} reporter facilitated study of the *Neurog3*$^{TA.LO}$ progenitor population.

Low Neurog3 protein levels promote a mitotic endocrine-biased Neurog3$^{TA.LO}$ *progenitor state*

Our new model is that abundant *Neurog3*$^{TA.LO}$ progenitors are maintained in a mitotic endocrine-biased state within plexus-state epithelial regions until they enter plexus-to-duct resolution (Bankaitis et al. 2015) using, in the interim, symmetric cell division to both maintain the endocrine-biased progenitor state and derive endocrine-committing *Neurog3*$^{TA.HI}$ cells. There was an apparent absence of asymmetric divisions that yield one *Neurog3*$^{TA.LO}$ and one *Neurog3*$^{TA.HI}$ daughter. Recently, Kim et al. (2015) published a real-time analysis of mitotic *Pdx1*^{GFP}- and *Neurog3*^{RFP}-expressing cells. They reported division events for *Pdx1*-expressing cells that were symmetric (for both progenitor renewal and terminal differentiation) and asymmetric (producing one Pdx1$^+$Sox9$^+$ daughter and one Neurog3$^+$ daughter). Similar to our observations, there was no asymmetric division for mitotic *Neurog3*-expressing cells. Furthermore, our results suggest that, at E12.5, perhaps connected to the rapid building and expansion of the incipient plexus-state epithelium occurring at this stage, the proportion of *Neurog3*$^{TA.LO}$ cells undergoing progenitor maintenance divisions relative to terminal differentiation events is higher than at E14.5. Limiting *Neurog3* expression in the strong hypomorphic condition increased the mitotic index of Sox9$^+$ *Neurog3*$^{TA.LO}$ progenitors and concurrently expanded their proportional representation within the epithelium at the expense of endocrine commitment (Fig. 6B,C), perhaps reflecting a shift in favor of progenitor-maintaining divisions. Recently, we reported that ablating *Neurog3* expression decreased the proliferation rate of the entire Sox9$^+$ epithelium (Bankaitis et al. 2015). Together, these studies support the idea that low Neurog3 protein levels are functionally associated with promoting progenitor-maintaining divisions, sustaining the actively cycling *Neurog3*$^{TA.LO}$ state (Fig. 7B). While reducing Neurog3 protein levels decreases endocrine biasing, particularly in the strong hypomorph context, its complete absence essentially totally ablates endocrine lineage potential (Gradwohl et al. 2000; Johansson et al. 2007; Wang et al. 2010). These observations indicate that the presence of low levels of Neurog3 protein is required to establish and maintain endocrine biasing, as opposed to commitment, in Sox9$^+$ *Neurog3*^{TA} cells.

Potentially important analogies can be drawn regarding these different behaviors driven by Neurog3 and the findings on how low versus high levels of Neurog2 maintain the cycling neural progenitor state or promote cell cycle exit and neural specification (Shimojo et al. 2008; Roybon et al. 2009; Ali et al. 2011; Florio et al. 2012). In those studies, *Neurog2*^{LO} cells were proliferative, while homozygous *Neurog2* inactivation stalled stem cell mitotic progression in the G1 phase, and overexpression accelerated cell cycle exit. In cycling progenitors, high Cdk activity and low Cdk inhibitor (Cdki) activity during G2–S–M phases keep Neurog2 in an unstable multiphosphorylated state subject to ubiquitylation-mediated degradation (Vosper et al. 2009; Ali et al. 2011). The low-level phospho-Neurog2 is unable to activate neural specification target genes but activates progenitor-associated targets (Ali et al. 2011; Hindley et al. 2012). In our case, the Sox9$^+$ *Neurog3*$^{TA.LO}$ population comprises cells with low to undetectable Neurog3 protein, and future experimentation could test for Sox9$^+$ *Neurog3*$^{TA.LO}$ progenitors containing low levels of an unstable phospho-Neurog3 protein that is periodically degraded during the cell cycle and is immunodetected, at least with current antibodies, in only a subset of the *Neurog3*-expressing Sox9$^+$ endocrine-biased cells. Neurog3 has been shown to be inherently unstable and subject to the same ubiquitylation-mediated degradation mechanisms as Neurog2 (Roark et al. 2012; Qu et al. 2013). These striking parallels for Neurog2 and Neurog3 predict that low levels of unstable Neurog3 activate a subset of target genes specifically associated with promoting progenitor maintenance and the endocrine-biased state. The low level of *Neurog3* expression in the endocrine progenitor context clearly has different consequences compared with the sustained low-level *Neurog3* expression in adult β cells that is necessary for physiological function: Neurog3 in mature β cells most likely activates target genes peculiar to quiescent endocrine cells (Wang et al. 2009).

Speculations on mechanisms regulating endocrine commitment vs. progenitor maintenance in Neurog3$^{TA.LO}$ *progenitors*

Several studies show that the length of the G1 phase of the cell cycle can dictate the choice of progenitor maintenance versus lineage specification (Hindley et al. 2012; Pauklin and Vallier 2013; Hardwick et al. 2015). For Neurog2 in neural progenitors, the low Cdk/high Cdki activity and lengthened G1 keep Neurog2 nonphosphorylated/underphosphorylated and stable enough to activate neuronal differentiation targets (Ali et al. 2011). Our model is that Neurog3 protein levels transition from low—sometimes immuno-undetectable but still present and functional—in cycling *Neurog3*$^{TA.LO}$ progenitors to uniformly high in endocrine-committing *Neurog3*$^{TA.HI}$ cells. Moreover, in every terminal differentiation division, we observed the irreversible transition to *Neurog3*$^{TA.HI}$ during what should be G1, ~3–6 h after parental *Neurog3*$^{TA.LO}$ cell mitosis (Fig. 4; Supplemental Table S3). Moreover, enforcing G1-like conditions with the Cdki p27Kip1 led to significantly increased Neurog3 stability

(Roark et al. 2012). In the Neurog3^{HI} state, Neurog3 promotes expression of the Cdki *Cdkn1a* (Miyatsuka et al. 2011), confirmed by our qRT–PCR analysis, creating a positive feed-forward loop driving cell cycle exit. If Neurog3 behaves like Neurog2, the G1 phase would be mechanistically coupled to Neurog3 accumulation for promoting the transition to endocrine lineage commitment.

We and others reported that altering *Neurog3* expression, along with affecting endocrine specification commitment, disturbs the morphological development and maintenance of the epithelial endocrine niche environment (Magenheim et al. 2011; Bankaitis et al. 2015). Therefore, a new viewpoint is emerging—that a vital part of learning how to manipulate endocrine progenitor states (for example, toward sustained in vitro production of endocrine cells of specific fates) will be to understand how the endocrine niche environment integrates intercellular signaling and cell-autonomous programs to regulate specification and commitment. Since Neurog3 protein levels critically regulate progenitor versus endocrine commitment, we judged it important to determine how Neurog3 protein stability and accumulation are regulated in Sox9^{+} *Neurog3*^{TA} progenitors. We were also interested in the possibility that intraepithelial *Neurog3* expression within the *Neurog3*$^{TA.LO}$ population, similar to the Hes1-dependent oscillation of *Neurog2* (Shimojo et al. 2008), undergoes dynamic oscillation between low-expressing and off states. Such oscillation might explain why Neurog3 protein falls below a detection threshold in many endocrine-biased progenitors as well as the cumulative labeling of the population using *R26R*-based lineage tracing. Investigating this issue would require novel *Neurog3*-driven reporters with the sensitivity to detect such dynamism. Characterizing these sorts of regulatory influences with increased spatiotemporal resolution could help to define how an endocrine specification commitment program is temporally deployed to generate the multilineage islets of Langerhans.

Materials and methods

Mice

Neurog3$^{BAC.Cre}$ [Tg(*Neurog3*-cre)C1Able/J] (Schonhoff et al. 2004) and *ROSA26R*^{EYFP} [B6.129 × 1-*Gt(ROSA)26Sor*$^{tm1(EYFP)Cos}$/J] (Srinivas et al. 2001) mice were described previously. *Neurog3*$^{EGFP/+}$ [B6.129.S-*Neurog3*$^{tm1(EGFP)Khk}$/Mmcd] (Lee et al. 2002) and *Neurog3*$^{FL/+}$ [*Neurog3*$^{tm1.1(cre/ERT)Ggu}$] (Wang et al. 2008) mice from Guoqiang Gu (Vanderbilt University) were described previously. All protocols were approved by the Vanderbilt University Institutional Animal Care and Use Committee. For genotyping primers, see Supplemental Table S5.

Immunodetection

Embryonic dorsal pancreata were fixed with 4% paraformaldehyde for 4–6 h at 4°C. Cryosectioning was done on sucrose-equilibrated (30% overnight at 4°C) OCT-embedded tissue (Tissue-Tek). A Leica CM3050S was used to cut 10-µm tissue sections, which were sequentially placed on three separate sets of slides, each covering ~33% of the dorsal pancreas. For primary and secondary antibodies, see Supplemental Table S4.

Flow sorting

Multiple E12.5 or E14.5 *Neurog3*$^{RG1+}$ dorsal pancreata were pooled and treated with Accumax (Sigma) for ~30–45 min (protocol available on request). Dispersed samples were washed and incubated on ice first with anti-Muc1 antibody for 1 h and then anti-hamster Cy5 secondary antibody for an additional hour. Samples were washed in cold PBS, and DAPI was added to ensure sorting of viable cells. Flow sorting was performed with a BD FACSAria III.

Static image acquisition and time-lapse movies

Unless noted, images are epifluorescence from a Zeiss ApoTome microscope with Zeiss Axiovision software. All scale bars indicate 20 µm. Confocal immunofluorescence images (Fig. 1H) and time-lapse movies were from a Zeiss LSM 510 confocal or LSM 780 two-photon microscope, respectively, analyzed with Zen 2.1 software. For time-lapse imaging, *Neurog3*$^{RG1+}$ explants were embedded in BD Matrigel (BD Biosciences) and imaged immediately or allowed to attach to bovine fibronectin (50 µg/mL) overnight before imaging. All pancreatic explants were cultured in DMEM (without phenol-red) with 10% FBS, penicillin, and streptomycin (10 U/mL each) at 37°C in an environmentally controlled chamber.

Acknowledgments

We thank Richard Behringer (Baylor College of Medicine) for the H2B^{mCherry}-peptide-2A-GFP^{GPI} reporter cassette. We thank Anna Means, Guoqiang Gu, Maureen Gannon, Roland Stein, Jake Kushner, and members of the Wright/Gu laboratories for discussions. This work used the Cell Imaging Shared Resource and Transgenic/Embryonic Stem Cell Shared Resource core facilities of the Vanderbilt Diabetes Research and Training Center funded by National Institute of Diabetes and Digestive and Kidney Diseases grant 020593. Flow cytometry was performed in the Vanderbilt University Medical Center Flow Cytometry Shared Resource supported by the Vanderbilt Ingram Cancer Center (P30 CA68485) and the Vanderbilt Digestive Disease Research Center (DK0558404). Generation of *Neurog3*^{RG1} mice was supported in part by the Beta Cell Biology Consortium Mouse Embryonic Stem Cell Core funded by the National Institute of Diabetes and Digestive and Kidney Diseases (U01DK072473). This study was supported by the National Institutes of Health/National Institute of Diabetes and Digestive and Kidney Diseases (U01DK089570) and an American Heart Association fellowship to M.E.B. (13POST14240011).

References

Ali F, Hindley C, McDowell G, Deibler R, Jones A, Kirschner M, Guillemot F, Philpott A. 2011. Cell cycle-regulated multi-site phosphorylation of Neurogenin 2 coordinates cell cycling with differentiation during neurogenesis. *Development* **138:** 4267–4277.

Bankaitis ED, Bechard ME, Wright CVE. 2015. Feedback control of growth, differentiation, and morphogenesis of pancreatic endocrine progenitors in an epithelial plexus niche. *Genes Dev* **29:** 2203–2216.

Bradford JA, Clarke ST. 2011. Dual-pulse labeling using 5-ethynyl-2′-deoxyuridine (Edu) and 5-bromo-2′-deoxyuridine (BrdU) in flow cytometry. *Curr Protoc Cytom* **55:** 7.38.1–7.38.15.

Cano DA, Soria B, Martin F, Rojas A. 2014. Transcriptional control of mammalian pancreas organogenesis. *Cell Mol Life Sci* **71:** 2383–2402.

Desgraz R, Herrera PL. 2009. Pancreatic neurogenin 3-expressing cells are unipotent islet precursors. *Development* **136:** 3567–3574.

De Vas MG, Kopp JL, Heliot C, Sander M, Cereghini S, Haumaitre C. 2015. Hnf1b controls pancreas morphogenesis and the generation of Ngn3$^+$ endocrine progenitors. *Development* **142:** 871–882.

Ejarque M, Cervantes S, Pujadas G, Tutusaus A, Sanchez L, Gasa R. 2013. Neurogenin3 cooperates with Foxa2 to autoactivate its own expression. *J Biol Chem* **288:** 11705–11717.

Florio M, Leto K, Muzio L, Tinterri A, Badaloni A, Croci L, Zordan P, Barili V, Albieri I, Guillemot F, et al. 2012. Neurogenin 2 regulates progenitor cell-cycle progression and Purkinje cell dendritogenesis in cerebellar development. *Development* **139:** 2308–2320.

Gradwohl G, Dierich A, LeMeur M, Guillemot F. 2000. Neurogenin3 is required for the development of the four endocrine cell lineages of the pancreas. *Proc Natl Acad Sci* **97:** 1607–1611.

Gu G, Dubauskaite J, Melton DA. 2002. Direct evidence for the pancreatic lineage: NGN3$^+$ cells are islet progenitors and are distinct from duct progenitors. *Development* **129:** 2447–2457.

Hardwick LJA, Ali FR, Azzarelli R, Philpott A. 2015. Cell cycle regulation of proliferation versus differentiation in the central nervous system. *Cell Tissue Res* **359:** 187–200.

Hindley C, Ali F, McDowell G, Cheng K, Jones A, Guillemot F, Philpott A. 2012. Post-translational modification of Ngn2 differentially affects transcription of distinct targets to regulate the balance between progenitor maintenance and differentiation. *Development* **139:** 1718–1723.

Johansson KA, Dursun U, Jordan N, Gu G, Beermann F, Gradwohl G, Grapin-Botton A. 2007. Temporal control of neurogenin3 activity in pancreas progenitors reveals competence windows for the generation of different endocrine cell types. *Dev Cell* **12:** 457–465.

Kim YH, Larsen HL, Rué P, Lemaire LA, Ferrer J, Grapin-Botton A. 2015. Cell cycle-dependent differentiation dynamics balances growth and endocrine differentiation in the pancreas. *PLOS Biol* **13:** e1002111.

Lee JC, Smith SB, Watada H, Lin J, Scheel D, Wang J, Mirmira RG, German MS. 2001. Regulation of the pancreatic pro-endocrine gene neurogenin3. *Diabetes* **50:** 928–936.

Lee CS, Perreault N, Brestelli JE, Kaestner KH. 2002. Neurogenin 3 is essential for the proper specification of gastric enteroendocrine cells and the maintenance of gastric epithelial cell identity. *Genes Dev* **16:** 1488–1497.

Magenheim J, Klein AM, Stanger BZ, Ashery-Padan R, Sosa-Pineda B, Gu G, Dor Y. 2011. Ngn3$^+$ endocrine progenitor cells control the fate and morphogenesis of pancreatic ductal epithelium. *Dev Biol* **359:** 26–36.

Miyatsuka T, Kosaka Y, Kim H, German MS. 2011. Neurogenin3 inhibits proliferation in endocrine progenitors by inducing Cdkn1a. *Proc Natl Acad Sci* **108:** 185–190.

Nimmo RA, May GE, Enver T. 2015. Primed and ready: understanding lineage commitment through single cell analysis. *Trends Cell Biol* **25:** 459–467.

Pan FC, Wright C. 2011. Pancreas organogenesis: from bud to plexus to gland. *Dev Dyn* **240:** 530–565.

Pauklin S, Vallier L. 2013. The cell-cycle state of stem cells determines cell fate propensity. *Cell* **155:** 135–147.

Puri S, Hebrok M. 2007. Dynamics of embryonic pancreas development using real-time imaging. *Dev Biol* **306:** 82–93.

Qu X, Afelik S, Jensen JN, Bukys MA, Kobberup S, Schmerr M, Xiao F, Nyeng P, Veronica Albertoni M, Grapin-Botton A, et al. 2013. Notch-mediated post-translational control of Ngn3 protein stability regulates pancreatic patterning and cell fate commitment. *Dev Biol* **376:** 1–12.

Roark R, Itzhaki L, Philpott A. 2012. Complex regulation controls Neurogenin3 proteolysis. *Biol Open* **1:** 1264–1272.

Roybon L, Hjalt T, Stott S, Guillemot F, Li J-Y, Brundin P. 2009. Neurogenin2 directs granule neuroblast production and amplification while NeuroD1 specifies neuronal fate during hippocampal neurogenesis. *PLoS One* **4:** e4779.

Schonhoff SE, Giel-Moloney M, Leiter AB. 2004. Neurogenin 3-expressing progenitor cells in the gastrointestinal tract differentiate into both endocrine and non-endocrine cell types. *Dev Biol* **270:** 443–454.

Seymour PA, Freude KK, Tran MN, Mayes EE, Jensen J, Kist R, Scherer G, Sander M. 2007. SOX9 is required for maintenance of the pancreatic progenitor cell pool. *Proc Natl Acad Sci* **104:** 1865–1870.

Shaner NC, Steinbach PA, Tsien RY. 2005. A guide to choosing fluorescent proteins. *Nat Methods* **2:** 905–909.

Shimojo H, Ohtsuka T, Kageyama R. 2008. Oscillations in notch signaling regulate maintenance of neural progenitors. *Neuron* **58:** 52–64.

Solar M, Cardalda C, Houbracken I, Martín M, Maestro MA, De Medts N, Xu X, Grau V, Heimberg H, Bouwens L, et al. 2009. Pancreatic exocrine duct cells give rise to insulin-producing β cells during embryogenesis but not after birth. *Dev Cell* **17:** 849–860.

Srinivas S, Watanabe T, Lin CS, William CM, Tanabe Y, Jessell TM, Costantini F. 2001. Cre reporter strains produced by targeted insertion of EYFP and ECFP into the ROSA26 locus. *BMC Dev Biol* **1:** 4.

Stephens DJ, Allan VJ. 2003. Light microscopy techniques for live cell imaging. *Science* **300:** 82–86.

Teta M, Rankin MM, Long SY, Stein GM, Kushner JA. 2007. Growth and regeneration of adult β cells does not involve specialized progenitors. *Dev Cell* **12:** 817–826.

Villasenor A, Chong DC, Cleaver O. 2008. Biphasic Ngn3 expression in the developing pancreas. *Dev Dyn* **237:** 3270–3279.

Vosper JMD, McDowell GS, Hindley CJ, Fiore-Heriche CS, Kucerova R, Horan I, Philpott A. 2009. Ubiquitylation on canonical and non-canonical sites targets the transciption factor neurogenin for ubiquitin-mediated proteolysis. *J Biol Chem* **284:** 15458–15468.

Wang S, Hecksher-Sorensen J, Xu Y, Zhao A, Dor Y, Rosenberg L, Serup P, Gu G. 2008. Myt1 and Ngn3 form a feed-forward expression loop to promote endocrine islet cell differentiation. *Dev Biol* **317:** 531–540.

Wang S, Jensen JN, Seymour PA, Hsu W, Dor Y, Sander M, Magnuson MA, Serup P, Gu G. 2009. Sustained Neurog3 expression in hormone-expressing islet cells is required for endocrine maturation and function. *Proc Natl Acad Sci* **106:** 9715–9720.

Wang S, Yan J, Anderson DA, Xu Y, Kanal MC, Cao Z, Wright CVE, Gu G. 2010. Neurog3 gene dosage regulates allocation of endocrine and exocrine cell fates in the developing mouse pancreas. *Dev Biol* **339:** 26–37.

Wilkinson G, Dennis D, Schuurmans C. 2013. Proneural genes in neocortical development. *Neuroscience* **253:** 256–273.

Zhang H, Tweedie E, Pope CF, Washington MK, Hipkens S, Means AL, Path G, Seufert J, Costa RH, Leiter AB, et al. 2009. Multiple, temporal-specific roles for HNF6 in pancreatic endocrine and ductal differentiation. *Mech Dev* **126:** 958–973.

Zhou Q, Law AC, Rajagopal J, Anderson WJ, Gray PA, Melton DA. 2007. A multipotent progenitor domain guides pancreatic organogenesis. *Dev Cell* **13:** 103–114.